This article has been accepted for publication in a future issue of this journal, but has not been fully edited. Content may change prior to final publication. Citation information: DOI 10.1109/TVT.2018.2840097, IEEE Transactions on Vehicular Technology

Influence Analysis of Typical Objects in Rural Railway Environments at 28 GHz

Danping He *Member, IEEE*, Bo Ai *Senior Member, IEEE*, Mathis Schmieder, Zhangdui Zhong *Senior Member, IEEE*, Junhyeong Kim, Bing Hui, Heesang Chung, Ilgyu Kim, Yang Hao *Fellow, IEEE*

***Abstract*—Millimeter wave (mmWave) is a key to realize high data-rate communication and enable smart railway services. There are more and more research work focusing on the algorithm and system design for railway communications in the mmWave band. A correct understanding of the mmWave channel characteristics for railway scenario is important to the estimation and evaluation of designed technologies. In this paper, the influence of typical objects in rural railway environment to the mmWave propagation channel is analyzed. Based on the channel measurement conducted at 28 GHz with train-to-infrastructure deployment in the rural railway environment, a ray tracing (RT) simulator is calibrated in terms of environment modeling and electromagnetic (EM) calculation. The dominant multi-path components of the measurement are tracked and matched with corresponding objects in the propagation environment. Accordingly, dominant propagation mechanisms (direct, penetration, reflection, scattering, etc.) are determined, the 3D environment model and the EM parameters of different objects are calibrated. To overcome the constraints of the measurement and analyze the influence more practically, the measurement campaign is extended to four different environment cases and four T2I deployments. With the predetermined dominant propagation mechanisms and calibrated EM parameters, reliable RT simulations are conducted. The influence of typical objects are analyzed for the considered environment cases and deployments. The analysis of this work not only helps to understand the important influential factors of propagation channel at the object level, but also can be useful in guiding deployment of mmWave communication system. The provided EM parameters and environment modeling suggestions will enable reliable RT based channel realization in rural railway environments.**

This work is supported by the NSFC under Grant (61771036, 61501021, and 61725101), Beijing Natural Science Foundation under Grant L161009 and L172020, State Key Lab of Rail Traffic Control and Safety Project under Grant RCS2017ZT008, Fundamental Research Funds for the Central Universities (2017JBM077 and 2017JBM010), and by Institute for Information & communications Technology Promotion(IITP) grant funded by the Korea government(MSIT) (No. B0115-16-0001, 5G Communication with a Heterogeneous, Agile Mobile network in the PyeongChang wInter Olympic competioN).

Danping He, Bo Ai and Zhangdui Zhong are with the State Key Laboratory of Rail Traffic Control and Safety, Beijing Jiaotong University, 100044, China, and also with Beijing Engineering Research Center of High-speed Railway Broadband Mobile Communications, 100044, China. (Corresponding author: Bo Ai, e-mail: boai@bjtu.edu.cn)

Mathis Schmieder is with the Wireless Communications and Networks Department, Fraunhofer Heinrich Hertz Institute, HHI, Berlin 10587, Germany. (e-mail: mathis.schmieder@hhi.fraunhofer.de)

Junhyeong Kim is with Mobile Application Research Department, Electronics and Telecommunications Research Institute (ETRI), Daejeon 34129, Korea and School of Electrical Engineering, Korea Advanced Institute of Science and Technology (KAIST), Daejeon 34141, Korea. (e-mail: jhkim41jf@kaist.ac.kr)

Bing Hui, Heesang Chung and Ilgyu Kim are with Future Mobile Communication Research Division, Electronics and Telecommunications Research Institute (ETRI), Daejeon 34129, Korea. (e-mail: huibing@etri.re.kr)

Yang Hao is with the School of Electronic Engineering and Computer Science, Queen Mary University of London, London E1 4NS, U.K.. (e-mail: y.hao@qmul.ac.uk)

***Index Terms*—Channel measurement, influence analysis, millimeter wave channel, railway communication, ray-tracing simulation**

I. Introduction

With larger under-utilized bandwidth than the sub-6 GHz bands, the millimeter-wave (mmWave) bands are important to high data-rate applications [1]–[6]. For the fifth-generation (5G) and future mobile communication, seamless connectivity and similar user experience is required no matter when the devices (UE) are still or moving [7]. The 'high speed' scenarios, in which the railway communications are included, have been put on the agenda of 3rd Generation Partnership Project (3GPP) [8] and International Telecommunication Union (ITU) [9]. "Train-to-infrastructure" (T2I), "Inter-wagon", "Intra-wagon", "Inside-the-station" and "Infrastructure-to-infrastructure" scenarios are the five future railway service defined in [10]. Among which, the mobility of T2I scenarios can be the highest and brings big challenges to communication systems [10]–[12]. The linear T2I deployment for 30 GHz band has been proposed in 3GPP [13], [14]. Horizon 2020 established 5GCHAMPION project [15] aiming to provide high-mobility broadband connections via 5G mmWave high capacity backhaul in 24 GHz-28 GHz. "Mobile Hotspot Network (MHN)" communication system is prototyped to support Gbps data rate services with a speed over 400 km/h [16].

As there are more and more research work focusing on designing technology and architecture for mmWave railway communication, correct understanding of the channel characteristics is important. The authors of [17] estimate and compare mmWave channel characteristics of both circular and rectangular tunnel scenarios via ray-tracing (RT) simulation. The work is then extended in [18] and [19]. At first, RT is calibrated by a limited field test of the MHN system in Seoul subway tunnel scenario. Based on which, channel characteristics of railway tunnel, urban and rural scenarios with straight and curved route shapes are studied [18]. In [19], the key channel parameters are analyzed and modeled for the MHN tunnel scenario at 25 GHz, and a 3GPP-like channel generator—Quadriga [20] is used to realize channel for railway scenario for the first time. In the 2016 Asia-Pacific Telecommunity (APT) meeting, T2I channel measurements at 40 GHz and 90 GHz in the viaduct scenario are presented [21]. The measured path losses (PLs) are fitted by close-in reference distance (CI) model, and the coefficients are reported less than the free space PL. Thereafter, the authors of [22] reconstruct

This article has been accepted for publication in a future issue of this journal, but has not been fully edited. Content may change prior to final publication. Citation information: DOI 10.1109/TVT.2018.2840097, IEEE Transactions on Vehicular Technology

the 3D environment model of the viaduct and calibrate RT by using the reported PL data at 90 GHz. The calibration result indicates that the side walls and the ground of the viaduct are the main factors that significantly impact the propagation channel. With similar channel modeling approach as [19], the authors of [23] conduct intensive reliable RT simulations on the calibrated environment model, and key parameters are provided for realizing 3GPP-like stochastic channel.

The aforementioned researches also imply that RT is a powerful tool not only for deterministic channel modeling, but also for bridging the gap between constrained channel measurements and the requirement of comprehensive parameters by stochastic channel models. As appropriate environment model and EM calculation are the keys towards reliable RT simulation, the study of the influence of the propagation environment at object/material level is important. A propagation measurement based influence analysis approach is proposed for the first time in our previous work [24], in which open space scenarios (urban, rural, cutting), tunnel and intra-wagon scenario are considered. Propagation measurements are conducted for certain materials found on typical railway objects, based on which, electromagnetic (EM) parameters are extracted and incorporated into RT. Monte Carlo analysis approach is used to generate enormous statistically consistent environment models and deployments for unbiased analysis, and significant objects of each scenario type are determined. As the considered random objects and materials of the open space scenarios are mainly from the buildings, more objects should be explored. Besides, as mentioned in the conclusion of [24], the work can be improved and validated with channel measurements in the practical railway environment.

In this paper, a channel measurement based influence analysis approach is proposed. The channel measurement is conducted at 28 GHz in a rural railway environment. The dominant multi-path components (MPCs) in the measurement are tracked. RT is used to identify the involved objects in the propagation environment and appropriate 3D environment model is obtained. The dominant propagation mechanisms are determined and the electromagnetic (EM) parameters of different objects are calibrated. To overcome the constraints of the measurement and analyze the influence more practically, the measurement campaign is extended to four different environment cases and four T2I deployments. With the selected mmWave propagation mechanisms (direct, penetration, reflection, scattering, etc.) and calibrated EM parameters, intensive reliable RT simulations are conducted on the extended scenarios. The influence of objects are analyzed and significant objects are determined. Compared with the work in [24], channel measurement in rural railway environment is involved, different situations are considered. There are significant changes in the calibrated EM parameters of tracks which results in very different influence on the propagation channel. Therefore, the work of this paper improves existing results by making adaptation to the determined significant objects. The provided EM parameters and suggestions on environment modeling will enable reliable RT based channel realization in rural railway environments. Moreover, the analysis of this work not only helps to understand the important influential factors of propagation channel at the object level, but also can be useful in guiding deployment of mmWave communication system.

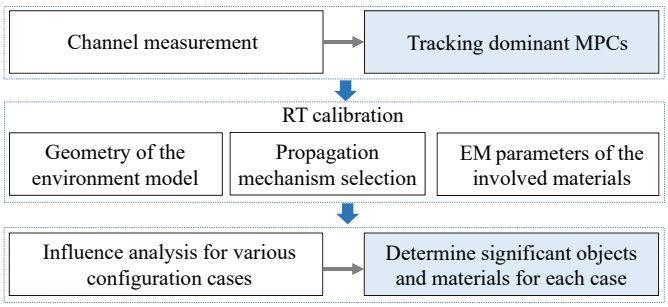

Figure 1: The proposed workflow

The remainder of this paper is organized as follows. The proposed workflow, the channel measurement and RT calibration are introduced in Section II. The influence of objects are analyzed for different environment cases with different deployments in Section III. Conclusions are drawn in Section IV.

II. The Proposed Workflow and Channel Measurement Based RT Calibration

The proposed workflow is shown in Fig. 1. Based on channel measurement in the considered environment, dominant MPCs can be tracked and matched to the corresponding objects in the target environment by using RT. Then, the geometry of the 3D environment model can be calibrated and the dominant propagation mechanisms are determined. By calibrating the EM parameters of the identified objects/materials, the reliability of RT simulations can be guaranteed. Thereafter, intensive RT simulations can be conducted with various transmitter (Tx)/ receiver (Rx) deployments as well as various combinations of the objects, which breaks the limits of the measurement. Based on the simulation results, the ray information are captured. The influence can be analyzed at the object level and their significances can be determined in the end. The workflow of this paper extends the framework proposed in [24] by employing the channel measurement based RT calibration. Both work together form a more comprehensive approach.

A. Measurement campaign of the T2I rural environment

The measurement is conducted by using a time-domain channel sounder. The hardware architecture is shown in Fig. 2. An FPGA-based signal generator provides the sounding signal at 3 GHz intermediate frequency (IF) with a bandwidth of 933 MHz, corresponding to a temporal resolution of about 1.1 ns. The IF signal is converted up to 28 GHz by mixing it with a local oscillator signal. The RF signal is then fed through a power amplifier and transmitted using a vertically polarized omni-directional antenna. At the Rx, a vertically polarized omni-directional antenna is used as well. Both the Tx and the Rx are synchronized using a high precision rubidium clock.

The measurement campaign is near a freight station with rural environment features, in Elstal, Germany. Several tracks are running in parallel. The measurement configuration is

This article has been accepted for publication in a future issue of this journal, but has not been fully edited. Content may change prior to final publication. Citation information: DOI 10.1109/TVT.2018.2840097, IEEE Transactions on Vehicular Technology

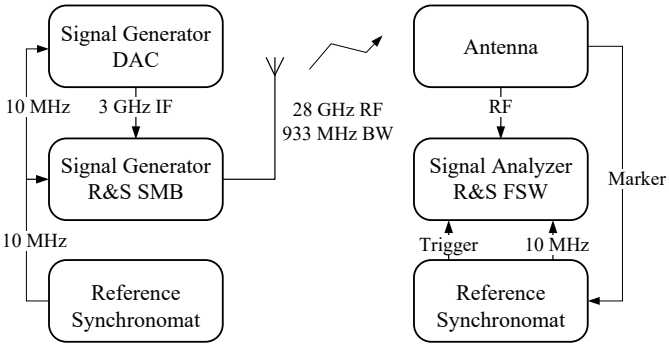

Figure 2: The overview of the hardware architecture of the channel sounder

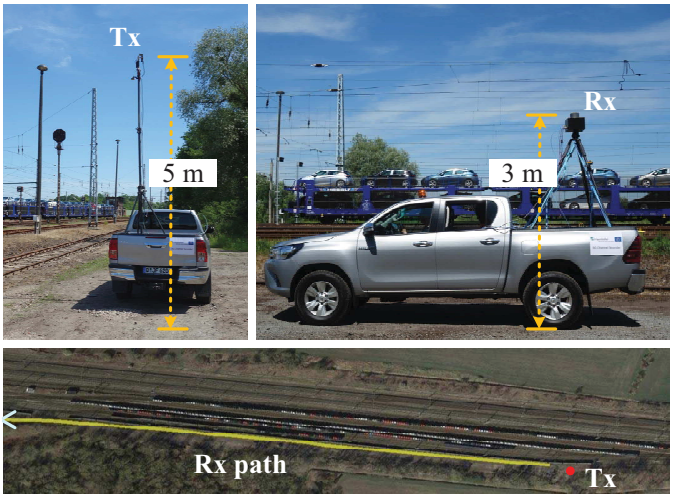

Figure 3: The Tx and Rx configurations in the measurement campaign

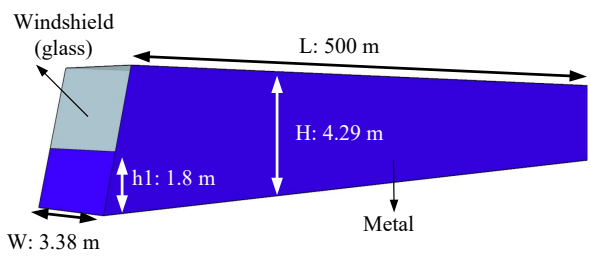

Figure 5: The 3D model of the train

shown in Fig. 3. Both the Tx and the Rx are placed on the beds of pick-up trucks. The amplifiers and antennas were mounted on tripods, allowing an easy adjustment of their heights. At the Tx, the antenna is fixed and the height is 5 m above ground. The Rx is placed with a height of 3 m. After the Tx and the Rx are calibrated using a back-to-back measurement, the Rx is moved with a constant speed around 1.75 m/s along a path beside the tracks. Fig. 3 shows the route map of the measured path, which is mainly line-of-sight (LoS) and one CIR snapshot is captured every 0.1 s. Table I summarizes the measurement setups.

Table I: Measurement setup

Center frequency	28 GHz
Bandwidth	933 MHz
Sampling rate at Rx	1120 MHz
Transmitting power	34 dBm
Tx height	5 m
Rx height	3 m
Tx-Rx distance	60 m - 550 m
Antenna type	Vertical polarization Omni-directional 0 dBi gain

B. RT calibration

1) MPC tracking and matching: Fig. 4(a) shows the details of the environment. There are catenary masts, ground, 8 tracks and a freight train at the furthest track. The width (W), height (H) and length (L) of the train are 3.38 m, 4.29 m, and 500 m, respectively, as shown in Fig. 5. The measured power delay profiles (PDPs) of all the snapshots are shown in Fig. 6(a). By considering a power threshold of -140 dBm, the trivial values and noises are ignored. The dominant MPCs are extracted from the peak values of the PDP. In average, 15 distinguishable and continuous MPCs are found in each snapshot. When the Rx goes further, the excess delays of all the MPCs reduce. MPC1 is the strongest with delay at 0 ns. MPC2 is nearly 0 ns, which can be generated by the object that is very close to the Tx and Rx. Besides, the MPC3-MPC14 appear with regular patterns: MPC3&4, MPC5&6, MPC7&8, $\cdots$, MPC13&14 are very close pairs. The average initial delay difference of the close MPCs is 9.7 ns. The difference of traveling distance is around 2.9 m, which is two times of the standard distance between two rails of a track. Therefore, despite the conclusion that the tracks are insignificant [24], the reconstructed 3D environment model of this scenario contains all the aforementioned objects, as shown in Fig. 4(b). The freight train, tracks and catenary mast are modeled as cuboid, and the ground is modeled as a rectangular plane. The geometry and assigned material names are summarized in Table II.

RT simulation is conducted with the same Tx and Rx configurations as the measurement. Direct path, up to 2nd order of reflections and diffuse scattering paths are considered. The delay, amplitude and 3D angles of the rays of each snapshot can be obtained after the simulation is finished. The rays that generated by the same surface are grouped. For each surface, the ray with the maximum amplitude is selected, and the evolution of those rays are shown in Fig. 6(b). As can be seen, the variations of the simulated MPCs match well with the measurement. According to the matching result, MPC1 contains the direct path, the 1st order reflection and diffuse scattering paths from the ground. As expected, MPC3-MPC18 are from the tracks and the involved propagation mechanism is diffuse scattering. MPC2 contains the diffused scattering rays from the ground, Track 1 and Track 2. MPC15 contains the 1st order reflection and diffuse scattering from the freight train.

2) Calibration of EM parameters: The RT calibration procedure of [18] is employed in this work to calibrate RT for all the snapshots. The calculation of the considered propagation mechanisms are summarized in Table. III. Fig. 6(c) compares

This article has been accepted for publication in a future issue of this journal, but has not been fully edited. Content may change prior to final publication. Citation information: DOI 10.1109/TVT.2018.2840097, IEEE Transactions on Vehicular Technology

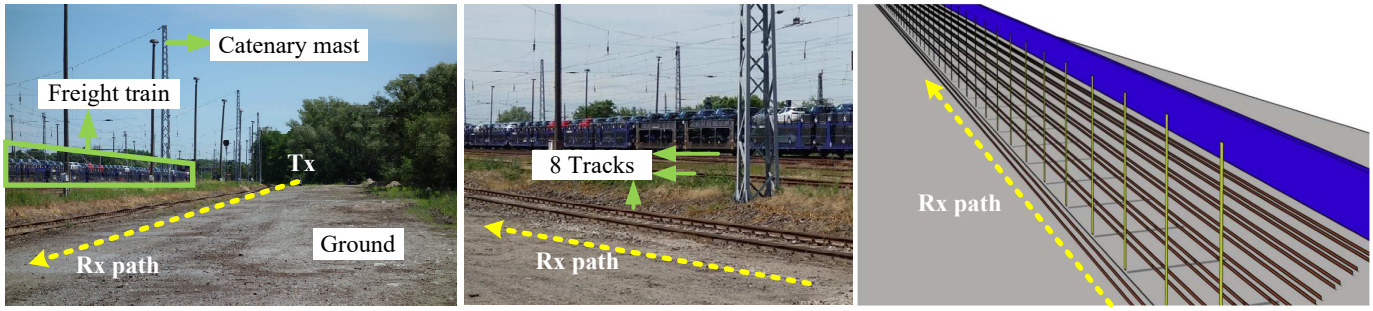

(a) Objects in the measured environments (b) Reconstructed environment model

Figure 4: The surrounding environment of the measurement campaign and the reconstructed 3D environment model

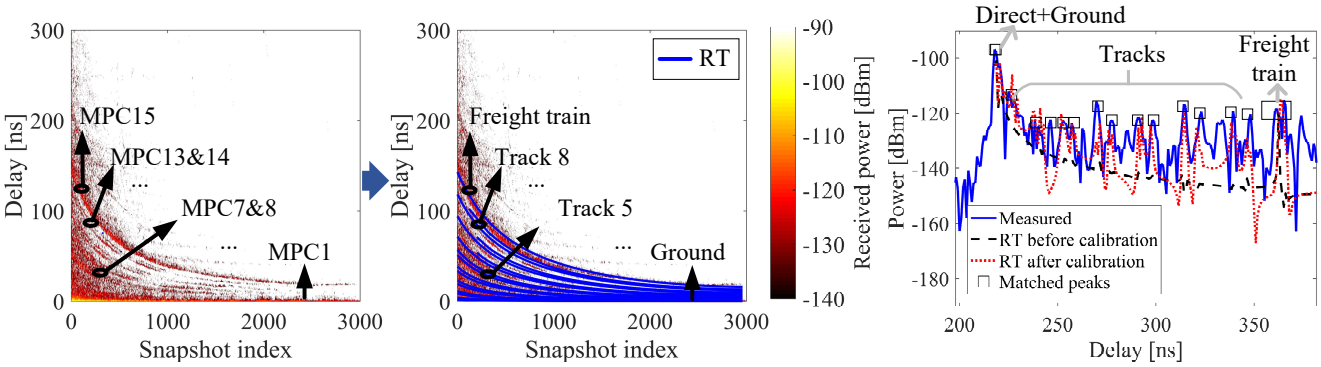

(a) (b) (c)

Figure 6: Tracking and calibration result of significant MPCs: (a) The measured PDP with power threshold -140 dBm and observed MPCs, (b) The tracked MPCs and corresponding objects from RT results, (c) The impulse response of snapshot 1.

Table II: Objects and corresponding materials in the considered environment

Object Name	Materials	Geometry
Train	Metal, glass	W: [3.2,3.4] m, L: [500,600] m, H: [4.2,5] m
Track	Metal	Distance between two rails (track width) d_r: 1.435 m, H: 0.18 m
Ground	Dry Soil with breakstone	Rectangle, H: 0 m
Catenary mast	Metal	Rectangle, W: 0.5 m, H: 12 m

the before and after calibration results for snapshot 1 as an example. Before the EM calibration, the reflected paths from the ground and the freight train almost reach the measured value, whereas the influence of tracks are underestimated, and the gaps of the MPC power from tracks between RT and the measurement is larger than 20 dB. After the calibration, the MPC power of tracks is increased and matches well with the measurement. The mean absolute error of MPC power of all the snapshots reduces from 12.33 dB to 3.26 dB, and the standard deviation of absolute errors reduces from 7.48 dB to 2.98 dB. Note that there are still a few unidentified peaks in this snapshot. The missing peaks are close to stronger peaks, which can be the diffuse scattering side lobe of the tracked objects (e.g. tracks, freight train) due to the irregular geometry at certain places, or can be the diffuse scattering from relatively smaller objects that are close to the modeled objects. Because the irregular geometrical variations and tiny non-typical objects do not always exist in the whole traveling path, they are not considered in the RT calibration and influence analysis in the current work.

The calibrated EM parameters are provided in Table IV.

Table III: Considered propagation mechanisms and corresponding calculation

Propagation	Geometry calculation	Electric field calculation
LOS	Free space LOS	Friis equation
Reflection	Snell's law with image-based method [25]	Fresnel equation [25]
Scattering	Directive scattering [26]	Scattering coefficient and equivalent roughness [26]

Compared with those before the calibration, the parameters of the ground and the catenary mast are unchanged. The S of the freight train and the track increases from 0.0015 to 0.0350 and 0.0650, respectively. Because the maximum scattering gain increases when S increases, the maximum scattering gain of the track is the largest, and that of the catenary mast is the smallest. The equivalent roughness of material reduces and the directional selectivity increases. Thus, the directional selectivity of the freight train is the strongest, and that of the track is the weakest. The α of the track decreases to 10, which is the smallest. As the α increases, the equivalent roughness of material reduces and the directional selectivity increases. Thus, the directional selectivity of the freight train and the catenary mast are very strong, and that of the track is the weakest.

This article has been accepted for publication in a future issue of this journal, but has not been fully edited. Content may change prior to final publication. Citation information: DOI 10.1109/TVT.2018.2840097, IEEE Transactions on Vehicular Technology

Table IV: Material parameters at 28 GHz

Object Name	Before Calibration				After Calibration			
	ϵ_r'	$tan\delta$	S	α	ϵ_r'	$tan\delta$	S	α
Ground	1.9212	0.2267	0.0025	24	1.9212	0.2267	0.0025	24
Freight train	1.0175	0.4807	0.0015	57	1.0175	0.4807	0.0350	50
Track	1.0175	0.4807	0.0015	57	1.0185	0.4907	0.0650	10
Catenary mast	1.0175	0.4807	0.0015	57	1.0175	0.4807	0.0015	57

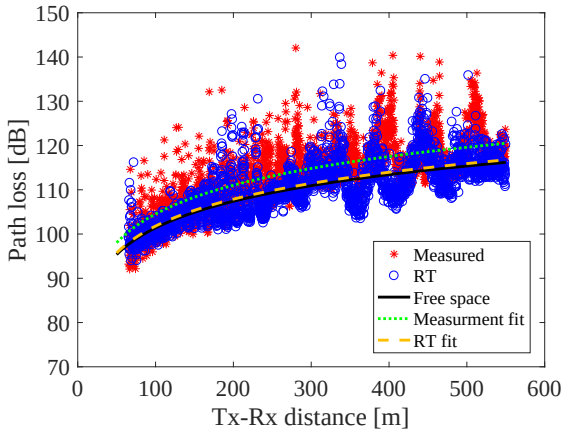

Figure 7: Comparison of the path loss between measurement and the calibrated RT result

Table V: Comparison of the PL between the calibrated RT and measurement

	Measurement	RT result	Difference
n	2.16	2.02	0.14
σ [dB]	4.80	4.26	0.60

The PLs of the measurement and the RT result are shown in Fig. 7. The mean absolute error and standard deviation absolute error of the simulated PL are 3.24 dB and 4.64 dB, respectively. The PLs are fitted by the single frequency CI model, which is expressed as:

$$PL(f_c, d)[dB] = FSPL(f_c, d_0)[dB] + 10nlog_{10}\left(\frac{d}{d_0}\right) + \chi_\sigma, \quad (1)$$

Where f_c is the center frequency, d is the Tx-Rx distance, d_0 is the reference distance, n is the path loss coefficient, χ_σ is the zero-mean Gaussian random variable with standard deviation σ. In this work, $d_0 = 1\ m$ and $d > d_0$, $FSPL(f_c, d_0)$ represents the free space path loss at d_0:

$$FSPL(f_c, d_0)[dB] = 20log_{10}\left(\frac{4\pi f_c}{c}\right), \quad (2)$$

Where $c = 3 \times 10^8$ m/s is the speed of light in air. The fitted parameters of the PL model are summarized in Table V. The differences of n and σ between the measurement and the simulation are 0.14 and 0.6 dB, respectively. According to the comparison in different aspects, the calibrated environment model, the selected propagation mechanisms and the calibrated material EM parameters together guarantee reliable RT simulations, which will be appropriate to realize propagation channels for similar rural railway environments.

III. Influence Analysis of Typical Objects

Although the conducted measurement is for the railway scenario with T2I configuration, the number of tracks in the rural scenario, which is far from a train station, is usually 2. Rather than always exists in the measurement campaign, the nearby train can occasionally pass by the train with Rx. Besides, due to the resource and policy constraints, the Rx in the measurement campaign is mounted on a car and the moving path is beside the tracks. Therefore, in order to make the analysis more practical and general, more scenarios with different deployments should be considered.

In this work, four different cases of the rural railway environment are defined and modeled, as can be seen in Fig. 8.

- **Case1** Two tracks: there are two tracks and the ground in the 3D model. The distance between the two track centers is 5.435 m, which is the same as that in the measurement campaign. This case is the most common seen in rural environments.
- **Case2** Multiple tracks: there are 8 tracks and the ground in the reconstructed model. The geometry parameters of the tracks are also the same as Case1. This case represents the rural railway environment near a train station.
- **Case3** Two tracks with a near passing by train: A passing by train is added on the second track. The size of the moving train that carries the Rx is the same as the freight train. This model represents the case when a train is passing by.
- **Case4** Multiple tracks with a far passing by train: A passing by train is added on the eighth track. This model represents the case near a train station, which is similar as the measurement campaign.

A moving train that carries the Rx is modeled with the same size as the train in Case3 and Case4. Note that, the windshield of the driving cabin is made of glass, and the radio wave can transmit with a constant penetration loss A_p, which ranges from 3 dB to 12 dB [18], [27], [28]. The starting height of the windshield glass is 1.8 m from the bottom of the train. The rest of the train body is assigned with the same material as the freight train in the measurement campaign.

The simulation parameters are summarized in Table VI. The antennas, transmitting power, considered frequency and the propagation mechanisms are the same as in the calibration. Note that the maximum observed reflection order in the RT calibration procedure is 1. In this work, the reflection order in the RT simulation is 2, which is sufficient to cover the considered environment cases with similar types of objects and geometrical compositions. The same material and the same calibrated EM parameters in Table IV are used. Besides, four different deployments (D1-D4) rather than the measured one are considered. The two-dimensional (2D) azimuth distance

This article has been accepted for publication in a future issue of this journal, but has not been fully edited. Content may change prior to final publication. Citation information: DOI 10.1109/TVT.2018.2840097, IEEE Transactions on Vehicular Technology

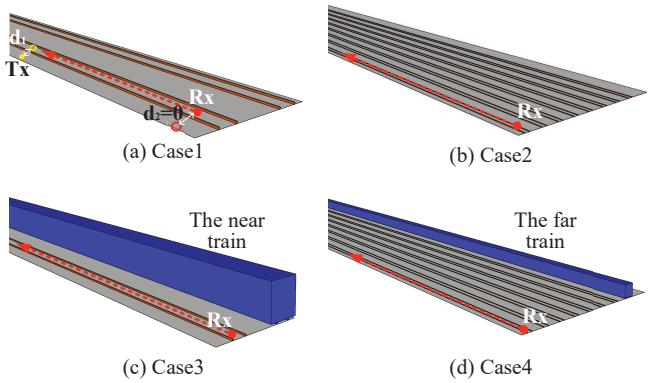

(a) Case1 (b) Case2 (c) Case3 (d) Case4

Figure 8: The 3D environment models of the four different cases

Table VI: Simulation parameters

Antenna type	Omni-directional, vertical polarization, 0 dBi	
Frequency	28 GHz	
Transmitting power	0 dBm	
Deployment and scenarios	**D1** (Tx: track side-Rx: on the top of the train), **D2** (Tx: over the track-Rx: on the top of the train), **D3** (Tx: track side-Rx: inside the driving cabin), **D4** (Tx: track side-Rx: in the front of the train) 4 deployments in each environment case	
Ray types	Direct	√
	Reflection bounces N_B	2
	Penetration	√
	Scattering	√

from the Tx to the track center with the moving train is denoted as d_1. The 2D azimuth distance from the Rx to the track center is denoted as d_2.

In D1, D3 and D4, the Tx is at the track side and the x-y-z coordinate is (0.5 m, 580 m, 5 m). d_1 is 2.22 m, which is shorter than the 2D distance between the catenary mast and the track. As a result, the propagation is line-of-sight, and there is always a direct path between the Tx and Rx. In D2, the Tx is mounted over the track with $d_1 = 0$ m, and the coordinate is (2.72 m, 580 m, 5 m). The Rx can be deployed on the top of the train (D1 and D2), inside the driving cabin D3, and in the front of the train (D4). For all the deployment, the Rx is over the track center and d_2 is 0 m. In D1 and D2, the coordinates of the starting and ending points of the Rx are (2.72 m, -0.2 m, 4.5 m) and (2.72 m, 549.8 m, 4.5 m), respectively. In D3, the starting and ending points of the Rx are (2.72 m, -0.1 m, 2.5 m) and (2.72 m, 549.9 m, 2.5 m), respectively. In D4, the starting and ending points of the Rx are (2.72 m, -0.01 m, 1.0 m) and (2.72 m, 550.01 m, 1.0 m), respectively. For each of the 4 cases, all the deployments are simulated. Therefore, the height of Rx in D4 is the smallest, and the heights of Rx in D1 and D2 are the largest. The moving length of Rx is 550 m with a step of 1 m. As a result, there are $N_s = 550$ snapshots in each deployment.

Some of the definitions and notations in [24] are used in this work. They are briefly introduced here for clarity. For each snapshot s, the RT results include the number of rays N_r, the type of a ray $T(s,j)$, bouncing times $B(s,j)$, hit objects $O(s,j)$ and complex field intensity $E(s,j)$ of ray j.

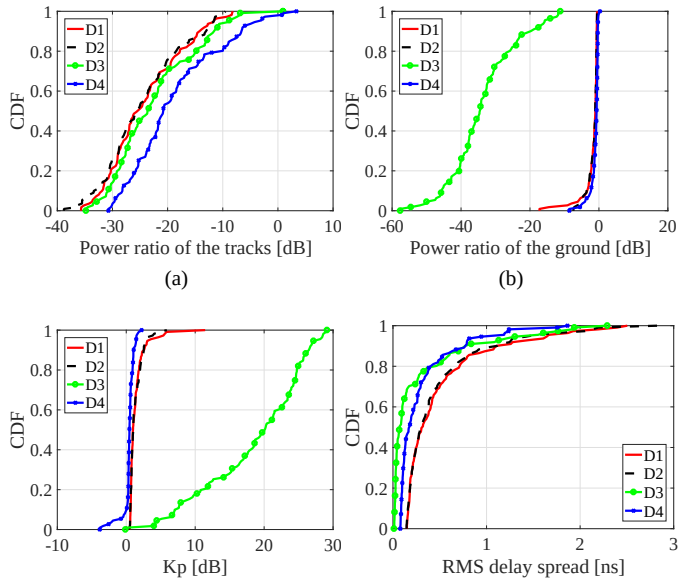

Figure 9: Results of Case1

The accumulated power of rays that hit object o is:

$$P_o(s) = |\sum_{j=1}^{N_r} C_j E(s,j)|^2 \tag{3}$$

where

$$C_j = \begin{cases} 1, & O(s,j) = o \\ 0, & else \end{cases} \tag{4}$$

The power ratio $R_o(s)$ of an object o in snapshot s in this work is expressed as $P_o(s)$ over the direct ray power $P_d(s)$ of the same snapshot.

$$R_o(s)[dB] = 10lg\left(\frac{P_o(s)}{P_d(s)}\right) \tag{5}$$

As P_o may be larger than P_m, R_o can be greater than 0 dB.

A. Case1: Two tracks

In this work, the same threshold -30 dB as in [24] is used in this work to distinguish the significant and insignificant objects. The CDFs of the power ratios of the tracks (R_{track}) are compared in Fig. 9(a). As can be seen, the mean R_{track}s of the 4 deployments are all greater than -30 dB. Table VII provides the mean power ratios of the considered objects for all the deployments in all the environment cases. When Rx is inside the cabin (D3) or on top of the train(D1 and D2), the significant scattering rays from the two tracks are obstructed by the moving train, and at lest 25% of the R_{track} below -30 dB. When the Rx is in the front of the train (D4), the scattering rays from the tracks are not obstructed. Therefore, the mean R_{track} of D4 (-20.8 dB) is the largest among all the deployments.

Fig. 9(b) compares the power ratios of the ground (R_{ground}). With least obstruction of the train body, the mean R_{ground} of D4 is the largest (-0.67 dB). According to the

This article has been accepted for publication in a future issue of this journal, but has not been fully edited. Content may change prior to final publication. Citation information: DOI 10.1109/TVT.2018.2840097, IEEE Transactions on Vehicular Technology

simulation result of all the deployments, the lower part of the driving cabin obstructs the reflected ray from the ground in all the snapshots, which explains the reason why the mean R_{ground} of D3 (-35 dB) is far less than that of the other deployments. When Rx is on top of the train (D1 and D2), there are more rays than D3, which come from the ground surfaces around the moving train, and the reflection is not always obstructed by the train body. Therefore, the mean R_{ground} of D1 and D2 are smaller than that of D4, and far greater than that of D3.

The power ratio of the direct path to the other MPCs K_p is studied in this work, and the expression is:

$$K_p(s) = \frac{P_d(s)}{\sum_{i=1}^{N_r} P(s,i) - P_d(s)} \tag{6}$$

Where $P(i)$ is the power of ray i, P_d is the power of the direct path. Thus, the purpose of K_p is to observe the power ratio at ray level.

Fig. 9(c) compares the K_ps of the 4 deployments. As the significant reflected rays from the ground are obstructed by the moving train body, the direct path dominates the power contribution. Therefore, the K_p of D3 is the largest (20 dB) among all the deployments. The mean K_ps of D1, D2 and D4 are slightly larger than 0 dB, indicating that with the reflection from the ground, the contribution of the other MPCs are comparable with the direct path.

The RMS delay spreads (DSs) are compared in Fig. 9(d). As the ground is the closest object to the Tx and the Rx, the path lengths of the strong MPCs from the ground are the closest to the direct path, which results in small excess delays. Therefore, the mean DSs of all the deployments are smaller than 0.3 ns. The DS of D3 is the smallest because reflected rays and many scattering rays from the ground and tracks are obstructed. Because the Rx of D1 and D2 are higher than that of D4, the path lengths of the MPCs are larger than D4, which results in larger mean DSs of D1 and D2. Table VIII provides the mean K_ps and DSs for all the deployments in all the environment cases.

B. Case2: Multiple tracks

Fig. 10 are the simulation results for Case2. Because more tracks exist in Case2, more scattering rays are generated. As can be seen in Fig. 10(a), R_{track}s of all the deployments increase compared with that in Case1. The increment of the mean R_{track} of D1 is 15.96 dB, whereas the increments of the others are less than 1 dB. Because the Tx of D2 is closer to all the tracks compared with D1 (Tx at the track side), the incident angle of the reflected ray is smaller in D2, resulting smaller reflectance of tracks than D1 at the same Rx locations. Furthermore, because the maximum scattering power is achieved at the reflection direction according to the directive scattering theory, the R_{track} in D1 increases much more significantly than D2 as the number of tracks increases. Besides, due to the blockage of the moving train body in D3 and the lower height in D4, less significant scattering rays from the tracks can arrive at the Rx. Therefore, the increase of R_{track} of D3 and D4 are much less than that of D1. The values

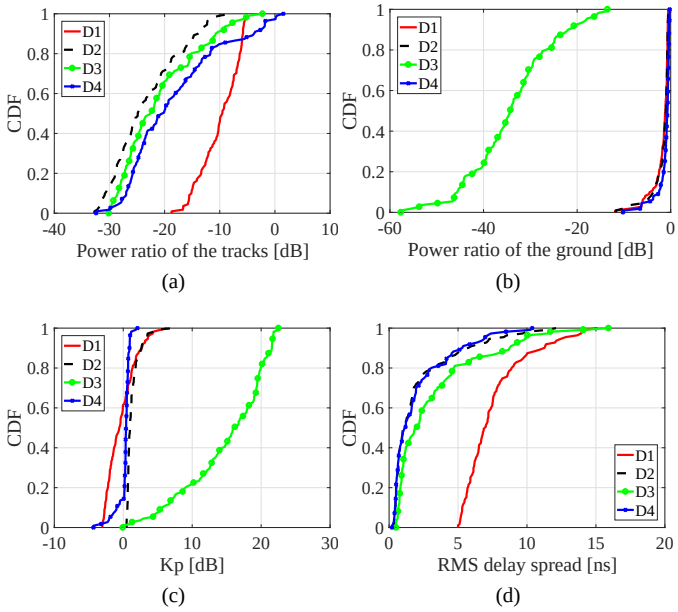

Figure 10: Results of Case2

Table VII: Power ratios of all the objects [dB]

		D1	D2	D3	D4
Case1	R_{track}	-25.48	-25.48	-23.65	-20.80
	R_{ground}	-1.04	-1.04	-34.55	-0.67
Case2	R_{track}	-9.52	-24.87	-22.60	-19.43
	R_{ground}	-1.12	-1.12	-34.34	-0.68
Case3	R_{track}	-26.10	-26.10	-24.30	-21.90
	R_{ground}	-1.06	-1.06	-35.96	-0.62
	R_{train}	-12.60	-2.14	0.10	1.04
Case4	R_{track}	-9.40	-25.60	-22.30	-16.69
	R_{ground}	-1.03	-1.03	-32.35	-0.69
	R_{train}	-17.64	-17.15	-12.00	-10.91

of R_{ground} of all the deployments are very similar as that in Case1 (see Fig. 10(b)), indicating that the increase of the track number does not have significant impact on the dominant rays generated by the ground.

Compared with Case1, the K_ps of all the deployments reduce due to the increased influence of tracks (see Fig. 10(c)). The K_p of D1 reduces from 1.01 dB to -0.55 dB, indicating that the accumulated contributions of the other MPCs are higher than the direct path.

The mean DSs of all the deployments increase to larger than 1.1 ns, and the DS of D1 is the largest (6.9 ns), indicating that the scattering rays from the far tracks have more significant contributions than the tracks near the moving train.

As the used EM parameters of the tracks are different in [24], the tracks are considered insignificant. However, the directive scattering coefficients of the tracks changes. S increases and α decreases, the tracks become significant objects to the propagation channel in the considered frequency band. As the EM parameteres of the ground is the same as that in [24], the ground is also significant object, which has a more significant impact than the tracks in the same deployment and the same environment.

This article has been accepted for publication in a future issue of this journal, but has not been fully edited. Content may change prior to final publication. Citation information: DOI 10.1109/TVT.2018.2840097, IEEE Transactions on Vehicular Technology

Table VIII: K_p and DS of all the cases

		D1	D2	D3	D4
Case1	K_p [dB]	1.01	1.01	20.07	0.46
	DS [ns]	0.31	0.31	0.07	0.17
Case2	K_p [dB]	-0.56	0.97	16.00	0.40
	DS [ns]	6.93	1.15	1.94	1.15
Case3	K_p [dB]	0.67	-1.34	3.14	-0.19
	DS [ns]	0.32	0.24	0.27	0.24
Case4	K_p [dB]	-0.60	0.82	8.60	-0.32
	DS [ns]	6.15	3.03	7.60	6.15

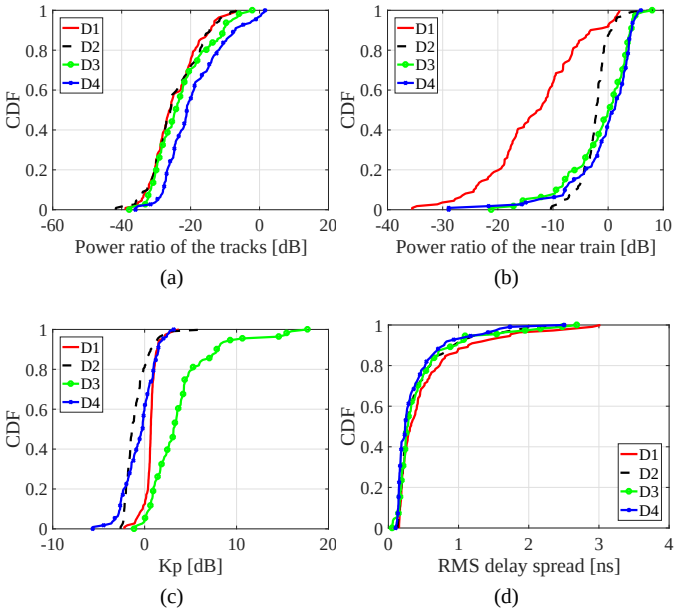

Figure 11: Results of Case3

C. Case3: Two tracks with a near passing by train

Due to the obstruction of the near train, the scattering rays from the tracks and ground are less than that in Case1, which makes the R_{track}s and R_{ground} slightly smaller than that of Case1, and the difference values are less than 1 dB. The power ratios of the near train R_{train} are shown in Fig. 11(b), the mean R_{train} of D3 and D4 approaches 0 dB. When Rx is on top of the train (D1 and D2), the height of Rx in D1 and D2 are higher than the nearby train. The less significant reflected and scattering rays arrive at the Rx, thus the mean R_{train}s are less than Rx in the front (D4) and inside driving cabin (D3). As the Tx of D1 is at the track side, the distances between the Tx and the near train surfaces are further than D2, and more area of the near train body are obstructed by the moving train body. As a result, the R_{train} of D1 is far less than that of D2. Besides, the R_{train} is larger than R_{track} in the same deployment.

With the similar reason as Case1 and Case2, K_p of D3 is the largest. However, because of the strong reflection and scattering from the near train, the mean K_p of D3 reduces to 3.2 dB, which is 16.8 dB and 12.8 dB less than Case1 and Case2, respectively. Due to the significant influence of the near train, the mean DSs of all the deployments are very similar to each other (around 0.3 ns). As a result, the near train has significant influence on the propagation channel. Its existence slightly reduces the power ratio of tracks and ground.

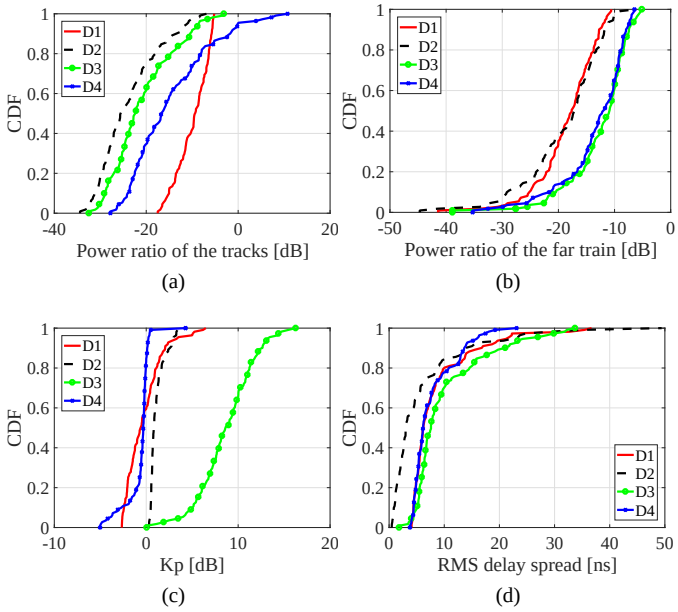

Figure 12: Results of Case4

D. Case4: Multiple tracks with a far passing by train

The power ratios of the tracks and the ground (Fig. 12(a)) in Case4 are similar as that in Case2. Therefore, the far train has trivial influence on the significance of the tracks and the ground. When the Rx is on top of the moving train (D1 and D2), less scattering rays arrive at the Rx compared with D3 and D4. As a result, the R_{train}s of D1 and D2 are less than that of D3 and D4 (see Fig. 12(b)), which is similar as in Case3. However, as the far train is further away from the Tx and Rx, the overall power ratios of the far train are smaller than in Case3. The difference between D1 and D2 reduces, as the visible parts of the far train are very similar in both deployments. As the mean power ratios of the tracks, far train and the ground are above -30 dB, they are significant objects in this case.

Because the visible area of the far train is smaller than the near train with D3 deployment, the K_p of D3 in Case4 is larger than that in Case3. Due to the additional contribution of the far train, the K_ps of Case4 are smaller than that of Case2. The DSs of all the deployments are larger than all the other cases. In D2 deployment, the ground contributes the most while the far train contributes the least to the propagation channel, the mean DS is the smallest. On the contrary, the mean DS of D3 is the largest.

E. Path loss

The path loss of the 4 cases are shown in Fig. 13. The parameters of the CI model are extracted for each deployment and each environment case, as summarized in Table IX. Note that the penetration loss of the train windshield in D3 is expressed as an offset in the CI model, therefore, it does not impact on n and σ. As can be seen, the σ of D3 in Case1 and Case2 are relatively small compared with the other cases, because many MPCs are obstructed by the moving train. The

This article has been accepted for publication in a future issue of this journal, but has not been fully edited. Content may change prior to final publication. Citation information: DOI 10.1109/TVT.2018.2840097, IEEE Transactions on Vehicular Technology

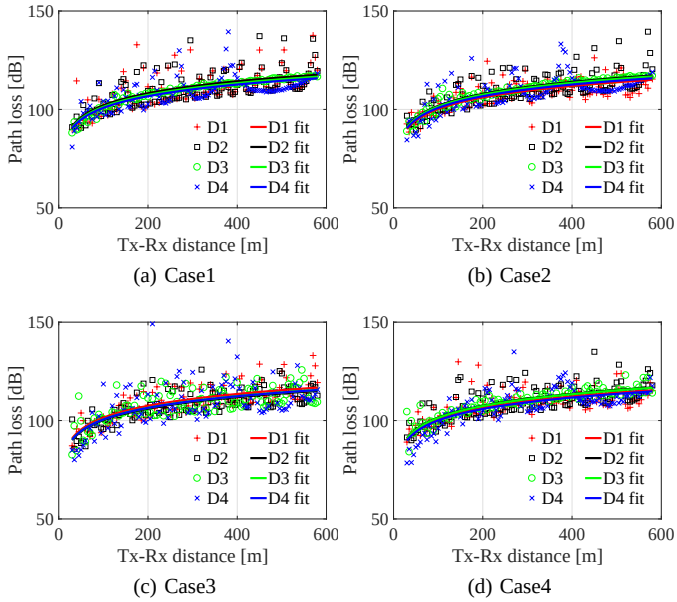

(a) Case1 (b) Case2 (c) Case3 (d) Case4

Figure 13: Path losses of the four cases

Table IX: Extracted parameters of PL model for all the cases

Case	D1		D2		D3		D4	
	n	σ [dB]	n	σ [dB]	n	σ [dB]	n	σ [dB]
Case1	2.03	7.07	2.03	6.82	2.00	1.26	1.97	5.93
Case2	1.94	4.82	2.02	6.08	2.00	1.71	1.97	6.17
Case3	2.00	5.50	1.94	5.08	1.96	5.36	1.96	8.67
Case4	1.95	5.60	2.01	5.99	2.00	2.58	1.93	5.88

path loss coefficients of D4 are all smaller than 2. Moreover, the DS of D4 is smaller than the other deployments in most of the cases. Thus, D4 is very likely to achieve better connection quality.

IV. Conclusion

In this paper, the influence of rural railway propagation environment and typical objects to the mmWave channel is analyzed. RT is used to track dominant MPCs in the measurement, identify the involved objects and calibrate the EM properties of the materials. The mean error and the standard deviation error of the calibrated MPCs is 3.26 dB and 2.98 dB, respectively. The small differences of PL parameters between the simulation and measurement indicate good matches. The study of extended environment cases and deployments via the calibrated RT overcomes the constraints of the measurement. It is observed that the tracks, and the passing by train are significant objects in all the considered cases and deployments. The ground is the most influential object except in D3 due to the obstruction of the moving train. The far passing by train contributes less than the near passing by train, and the existence of the passing by train does not significantly change the influence of the tracks and the ground. When the Rx is lower and in the front of the train (D4), the PL and DS are smaller than the other deployments in most of the cases. Thus, D4 is very likely to achieve better connection quality. The provided EM parameters and suggestions on environment modeling will enable reliable RT based channel realization in rural railway environments. Moreover, the analysis of this work not only helps to understand the important influential factors of propagation channel at the object level, but also can be useful in guiding deployment of mmWave communication system in similar environments.

References

[1] X. Wu, C. X. Wang, J. Sun *et al.*, "60-GHz millimeter-wave channel measurements and modeling for indoor office environments," *IEEE Transactions on Antennas and Propagation*, vol. 65, no. 4, pp. 1912–1924, Apr. 2017.

[2] W. Fan, I. Carton, J. Ø. Nielsen *et al.*, "Measured wideband characteristics of indoor channels at centimetric and millimetric bands," *EURASIP Journal on Wireless Communications and Networking*, vol. 2016, no. 1, p. 58, Feb. 2016.

[3] B. Ai, K. Guan, R. He *et al.*, "On indoor millimeter wave massive mimo channels: Measurement and simulation," *IEEE Journal on Selected Areas in Communications*, vol. 35, no. 7, pp. 1678–1690, Jul. 2017.

[4] T. S. Rappaport, Y. Xing, G. R. MacCartney *et al.*, "Overview of millimeter wave communications for fifth-generation (5G) wireless networks-with a focus on propagation models," *IEEE Transactions on Antennas and Propagation*, vol. 65, no. 12, pp. 6213–6230, Dec. 2017.

[5] S. Hur, S. Baek, B. Kim *et al.*, "Proposal on millimeter-wave channel modeling for 5G cellular system," *IEEE Journal of Selected Topics in Signal Processing*, vol. 10, no. 3, pp. 454–469, Apr. 2016.

[6] J. Zhang, P. Tang, L. Tian *et al.*, "6–100 GHz research progress and challenges from a channel perspective for fifth generation (5G) and future wireless communication," *Science China Information Sciences*, vol. 60, no. 8, pp. 1–16, Aug. 2017.

[7] K. Guan, G. Li, T. Kürner *et al.*, "On millimeter wave and THz mobile radio channel for smart rail mobility," *IEEE Transactions on Vehicular Technology*, vol. 66, no. 7, pp. 5658–5674, Nov. 2016.

[8] "Study on scenarios and requirements for next generation access technologies (Release 14)," *3rd Generation Partnership Project (3GPP) TR 38.913-14.3.0*, Aug. 2017.

[9] "IMT vision - framework and overall objectives of the future development of IMT for 2020 and beyond," *Recommendation ITU-R M.2083-0*, Sep. 2015.

[10] B. Ai, K. Guan, M. Rupp *et al.*, "Future railway services-oriented mobile communications network," *IEEE Communications Magazine*, vol. 53, no. 10, pp. 78–85, Oct. 2015.

[11] J. Moreno, J. Riera, L. De Haro *et al.*, "A survey on future railway radio communications services: challenges and opportunities," *IEEE Communications Magazine*, vol. 53, no. 10, pp. 62–68, October 2015.

[12] B. Ai, X. Cheng, T. Kürner *et al.*, "Challenges toward wireless communications for high-speed railway," *IEEE Transactions on Intelligent Transportation Systems*, vol. 15, no. 5, pp. 2143–2158, 2014.

[13] Mitsubishi Electric and ETRI, "R1-165484 WF on evaluation assumption for high speed-train scenario 30GHz," *3rd Generation Partnership Project (3GPP) RAN1#85*, May 2016.

[14] Mitsubishi Electric, ETRI, and Ericsson, "R1-165926 WF on additional evaluation assumptions for high speed train scenario: Macro + relay around 30GHz," *3rd Generation Partnership Project (3GPP) RAN1#85*, May 2016.

[15] E. C. Strinati, A. Clemente, J. Pajunpaa *et al.*, "Deliverable D1.2: First period report," *5GCHAMPION Project*, Jun. 2017. [Online]. Available: http://www.5g-champion.eu/Pages/DELIVERABLES.aspx

[16] J. Kim and I. G. Kim, "Distributed antenna system-based millimeter-wave mobile broadband communication system for high speed trains," in *2013 International Conference on ICT Convergence (ICTC)*, Oct. 2013, pp. 218–222.

[17] G. Li, B. Ai, K. Guan *et al.*, "Channel characterization for mobile hotspot network in subway tunnels at 30 GHz band," in *2016 IEEE 83rd Vehicular Technology Conference (VTC Spring)*, May 2016, pp. 1–5.

[18] D. He, B. Ai, K. Guan *et al.*, "Channel measurement, simulation, and analysis for high-speed railway communications in 5G millimeter-wave band," *IEEE Transactions on Intelligent Transportation Systems*, vol. PP, no. 99, pp. 1–15, Dec. 2017.

[19] ——, "Stochastic channel modeling for railway tunnel scenarios at 25 GHz," *ETRI Journal*, vol. 40, no. 1, pp. 39–50, Feb. 2018. [Online]. Available: http://dx.doi.org/10.4218/etrij.2017-0190

This article has been accepted for publication in a future issue of this journal, but has not been fully edited. Content may change prior to final publication. Citation information: DOI 10.1109/TVT.2018.2840097, IEEE Transactions on Vehicular Technology

[20] S. Jaeckel, L. Raschkowski, K. Börner *et al.*, "QuaDRiGa: A 3-D multi-cell channel model with time evolution for enabling virtual field trials," *IEEE Transactions on Antennas and Propagation*, vol. 62, no. 6, pp. 3242–3256, June 2014.

[21] T. Kawanishi, A. Kanno, H. Ogawa *et al.*, "Proposal of a new working document of a draft new apt report on millimeter-wave band railway radiocommunication systems between train and trackside, and its work plan," in *the 20th meeting of the APT Wireless Group (AWG-20)*, Sep. 2016.

[22] X. Lin, B. Ai, D. He *et al.*, "Measurement based ray tracer calibration and channel analysis for high-speed railway viaduct scenario at 93.2 GHz," in *2017 IEEE International Symposium on Antennas and Propagation USNC/URSI National Radio Science Meeting*, July 2017, pp. 617–618.

[23] L. Wang, B. Ai, K. Guan *et al.*, "Stochastic channel modeling for high-speed railway viaduct scenario at 93.2 GHz," in *2018 12th European Conference on Antennas and Propagation (EUCAP)*, Apr. 2018, pp. 1–1.

[24] D. He, B. Ai, K. Guan *et al.*, "Influence of typical railway objects in mmwave propagation channel," *IEEE Transactions on Vehicular Technology*, vol. PP, no. 99, pp. 1–1, Dec. 2017.

[25] A. S. Glassner, Ed., *An Introduction to Ray Tracing*. London, UK, UK: Academic Press Ltd., 1989.

[26] V. Degli-Esposti, F. Fuschini, E. M. Vitucci *et al.*, "Measurement and modelling of scattering from buildings," *IEEE Transactions on Antennas and Propagation*, vol. 55, no. 1, pp. 143–153, Jan. 2007.

[27] M. Lerch, P. Svoboda, S. Ojak *et al.*, "Distributed measurements of the penetration loss of railroad cars," in *2017 IEEE 86th Vehicular Technology Conference (VTC-Fall)*, Sept. 2017, pp. 1–5.

[28] T. Berisha, P. Svoboda, S. Ojak *et al.*, "Seghyper: Segmentation- and hypothesis based network performance evaluation for high speed train users," in *2017 IEEE International Conference on Communications (ICC)*, May 2017, pp. 1–6.

Danping He (M'16) received B.E. degree from Huazhong University of Science and Technology in 2008, M.Sc. degree from the Universite Catholique de Louvain (UCL) and Politecnico di Torino (PdT) in 2010, and Ph.D. degree from Universidad Politécnica de Madrid in 2014. In 2012, she was a visiting scholar in Institut national de recherche en informatique et en automatique, France. She worked in Huawei Technologies from 2014 to 2015 as a research engineer, and she is currently conducting postdoctoral research in the State Key Laboratory of Rail Traffic Control and Safety, Beijing Jiaotong University.

She has authored/co-authored more than 40 papers, 3 patents and 1 IEEE standard. Her papers received 5 Best Paper Awards. Her current research interests include radio propagation and channel modeling, ray tracing simulator development and wireless communication algorithm design.

Bo Ai (M'00-SM'10) received his Master and Ph.D. degree from Xidian University in 2002 and 2004 in China, respectively. He graduated in 2007 with great honors of Excellent Postdoctoral Research Fellow in Tsinghua University. He is now working in Beijing Jiaotong University as a professor and advisor of Ph.D. candidates. He is a deputy director of State Key Lab of Rail Traffic Control and Safety. He is an associate editor for IEEE Trans. on Consumer Electronics and an editorial committee member of journal of Wireless Personal Communications.

He has authored/co-authored 6 books, 140 scientific research papers and 26 invention patents in his research area till now. His current interests are the research and applications OFDM techniques, HPA linearization techniques, radio propagation and channel modeling, GSM for railway systems, and LTE for railway systems. He is an IET Fellow and an IEEE Senior member.

Mathis Schmieder received his B.S. and M.S. degrees in Electrical Engineering from the Technical University of Berlin, Germany, in 2012 and 2017, respectively. Since then, he has been with the Fraunhofer Heinrich-Hertz-Institute in Berlin, Germany. He is also currently pursuing his Ph.D. degree at TU Berlin. His main research interests include millimeter-wave communications, measurement and modelling of wireless propagation channels and wireless systems and transceiver architectures with emphasis on RF and mixed-signal circuit design.

Zhangdui Zhong (SM'16) is a professor and advisor of Ph.D. candidates in Beijing Jiaotong University. He is now a director of School of Computer and Information Technology and a Chief Scientist of State Key Laboratory of Rail Traffic Control and Safety in Beijing Jiaotong University. He is also a director of the Innovative Research Team of Ministry of Education, and a Chief Scientist of Ministry of Railways in China. He is an executive council member of Radio Association of China, and a deputy director of Radio Association of Beijing. His interests are wireless communications for railways, control theory and techniques for railways, and GSM-R system. His research has been widely used in the railway engineering, such as Qinghai-Xizang railway, Datong-Qinhuangdao Heavy Haul railway, and many high-speed railway lines of China.

He has authored/co-authored 7 books, 5 invention patents, and over 200 scientific research papers in his research area. He received MaoYiSheng Scientific Award of China, ZhanTianYou Railway Honorary Award of China, and Top 10 Science/Technology Achievements Award of Chinese Universities.

Junhyeong Kim received his B.S. degree in Department of Electronic Engineering from Tsinghua University, Beijing, China, in 2008, and M.S. degree in Department of Electrical Engineering from Korea Advanced Institute of Science and Technology (KAIST), Korea, in 2011. Since 2011, he has been with Electronics and Telecommunications Research Institute (ETRI), Korea. He is also currently pursuing his Ph.D. degree in School of Electrical Engineering at KAIST. His main research interests include millimeter-wave communications, MIMO, cooperative communications and handover.

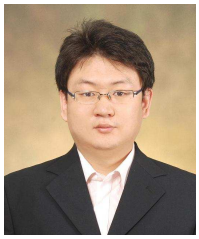

Bing Hui received his B.S. degree in communication engineering from Northeastern University, Shenyang, China, in 2005. He received his M.Eng. degree and Ph.D. degree at the Graduate School of Information Technology and Telecommunications, Inha University, Incheon, Rep. of Korea, in 2009 and 2013 respectively. He was with the Electronic Engineering Department, Inha University, Incheon, Korea as a Postdoctoral research fellow from 2013 to 2014. Since 2014, he has been working as a Researcher in the Electronics and Telecommunications Research Institute (ETRI), Daejeon, Rep. of Korea. His research interests include the 3GPP LTE(-A)/5G systems, mmWave mobile wireless backhauling, MIMO techniques, optimal codebook design, and mobile Ad-Hoc networks.

This article has been accepted for publication in a future issue of this journal, but has not been fully edited. Content may change prior to final publication. Citation information: DOI 10.1109/TVT.2018.2840097, IEEE Transactions on Vehicular Technology

Heesang Chung received the bachelor's degree in physics from Korea Advanced Institute of Science and Technology, Daejeon, Rep. of Korea, in 1993, and the MS and PhD degrees from Chungnam National University, Daejeon, Rep. of Korea, in 1995 and 1999, respectively. Since then, he has been with Electronics and Telecommunications Research Institute where he is currently the Principal Researcher. His career in ETRI began with the optical communications, and moved on to the mobile and wireless communication systems in 2005. He had involved in research projects related to LTE and LTE-Advanced from 2006 to 2010. His recent research interests are in 5G with special emphasis on high data-rate services for passengers on public transportations such as the buses, subway and bullet trains.

Ilgyu Kim received the BS and MS degree in electronic engineering from University of Seoul, Seoul, Rep. of Korea, in 1993 and 1995, and his PhD degree in Information Communications Engineering from Korea Advanced Institute of Science and Technology, Daejeon, Rep. of Korea, 2009. Since 2000, he has been with Electronics and Telecommunications Research Institute, where he has been involved in the development of WCDMA, LTE and MHN systems. Since 2012, he is the leader of the mobile wireless backhaul research section. His main research interests include millimeter wave communications and 5G mobile communications.

Yang Hao (M'00-SM'06-F'13) received the Ph.D. degree on computational electromagnetics from the Centre for Communications Research (CCR) at University of Bristol, U.K., in 1998.

He is currently a Professor of antennas and electromagnetics in the Antenna Engineering Group, Queen Mary, University of London. Prior to his appointment at Queen Mary, he was a postdoc research fellow at School of Electronic, Electrical and Computer Engineering, University of Birmingham.

Over the years, Professor Hao developed several fully-integrated antenna solutions based on novel artificial materials to reduce mutual RF interference, weight, cost and system complexity for security, aerospace and healthcare. He developed, with leading UK industries, novel and emergent gradient index materials to reduce mass, footprint and profile of low frequency and broadband antennas. He also co-developed the first stable active non-Foster metamaterial to enhance usability through small antenna size, high directivity, and tuneable operational frequency. He coined the term Body-centric wireless communications, i.e. networking among wearable and implantable wireless sensors on the human body. He was the first to characterize and include the human body as a communication medium between on-body sensors using surface and creeping waves. He contributed to the industrial development of the first wireless sensors for healthcare monitoring. Professor Hao is a strategic advisory board member for Engineering and Physical Sciences Research Council (EPSRC), where he is committed to championing RF/microwave engineering for reshaping the future of UK manufacturing and electronics.

Professor Hao is active in a number of areas, including computational electromagnetics, microwave metamaterials, graphene and nanomicrowaves, antennas and radio propagation for body centric wireless networks, active antennas for millimeter/sub-millimeter applications and photonic integrated antennas. Professor Hao has published over 140 journal papers and he was a co-editor and co-author of the books Antennas and Radio Propagation for Body-Centric Wireless Communications (Boston, MA, USA: Artech House, 2006, 2012), and FDTD Modelling of Metamaterials: Theory and Applications (Boston, MA, USA: Artech House, 2008), respectively.

Prof. Hao is currently a founding editor-in-chief of EPJ-AM, a new open access journal devoted to applied metamaterials research. He was an Editor-in-Chief of IEEE Antennas and Propagation Letters during 2013-2017. He was an Associate Editor of the same journal, IEEE Transactions on Antennas and Propagation during 2008-2013, and also a Co-Guest Editor for the IEEE Transactions on Antennas and Propagation in 2009. Professor Hao is a member of Board of the European School of Antenna Excellence, a member of EU VISTA Cost Action and the Virtual Institute for Artificial Electromagnetic Materials and Metamaterials, Metamorphose VI AISBL. He was a Vice Chairman of the Executive Team of IET Antennas and Propagation Professional Network. Professor Hao has published more than 120 journal papers and served as an invited and keynote speaker, conference General Chair, session chair and short course organizer at many international conferences. He won IET AF Harvey Research Prize in 2016, BAE Chairmans Silver award in 2014 and the Royal Society Wolfson Research Merit Award in 2012. Professor Hao was elected as a Fellow of the ERA Foundation in 2007, Fellow of the IET in 2010 and Fellow of the IEEE in 2013.